ITS-90 CALIBRATION OF RADIOMETERS USING WIRE/THIN-FILM THERMOCOUPLES IN THE NIST RTP TOOL: EFFECTIVE EMISSIVITY MODELING

B.K. Tsai and D.P. DeWitt
Optical Technology Division
National Institute of Standards and Technology
100 Bureau Drive Stop 8441
Gaithersburg, MD 20899-8441 USA

Models were developed to estimate the wafer effective emissivity as a function of the optical properties and geometrical configuration of the wafer and chamber in the NIST Rapid Thermal Processing (RTP) tool. These estimates were used to determine wafer temperatures from observed spectral radiance temperatures obtained with a light-pipe radiation thermometer (LPRT) calibrated on the International Temperature Scale of 1990 (ITS-90) against a blackbody. Out of the total uncertainty of 3.5 °C for the LPRT temperature measurements, the uncertainty component due to the effective emissivity uncertainty contributed about 2.0 °C. (In this paper all uncertainties are reported with a coverage factor of $k = 1$.) The model-corrected LPRT temperature measurements were in agreement with measurements using the new NIST combination wire/thin-film thermocouples (TC) calibrated against the ITS-90 with an uncertainty of less than 0.4 °C for the wafer temperature range 700 °C to 900 °C.

INTRODUCTION

Our companion paper [1] demonstrated an *in-situ* method for calibrating light-pipe radiation thermometers (LPRTs) to the International Temperature Scale of 1990 (ITS-90). New combination wire/thin-film thermocouples (TCs) were calibrated against the ITS-90 with an uncertainty of less than 0.4 °C (all uncertainties referred to here have a coverage factor of $k = 1$). Viewing a target on a silicon test wafer mounted within the NIST Rapid Thermal Processing (RTP) tool, the LPRTs were calibrated against the TCs with an uncertainty of less than 2.1 °C for the range 650 °C to 920 °C. The largest contribution to the measurement uncertainty (2.0 °C; see Table 1 of [1]) in the calibration process is due to the temperature gradient over the separation distance between the TC thin-film sensing junctions and the LPRT target. The uncertainty contribution from the LPRT calibration against a blackbody is about 0.2 °C [2], while that depending upon performance (noise in the RTP environment) is about 0.3 °C. It is important to recognize that, for this situation, the TC and LPRT calibration uncertainties are of similar value (0.4 °C and 0.3 °C, respectively), but because of the conditions within the tool, the uncertainty associated with the LPRT measurements will necessarily be much higher. The calibration of the LPRT against the TCs in the tool is restricted to the conditions of the comparison, namely, for a wafer of the same emissivity and the wafer-chamber arrangement of the tool.

For the chamber arrangement with the specular, highly reflecting (99.3 %) shield, and a 12.5-mm gap spacing between the wafer and shield (see Figure 1[1]), the LPRT spectral radiance temperature measurements are about 3 °C lower than those for the TFTCs. This difference is primarily due to the low emissivity of the wafer (0.65 at 800 °C) and would decrease as the wafer surface emissivity increases. The wafer-chamber arrangement formed by the hot wafer and cold reflective shield approximates a 2-surface (infinite-parallel planes) enclosure that enhances the wafer emissivity. Even though the reflecting shield is exceptionally close to unity, the LPRT indicates a spectral radiance temperature T_l that is several degrees below the wafer temperature T. In order to reduce the uncertainty of the LPRT calibration to determine wafer temperature, it is necessary to build a model of the wafer-chamber arrangement to estimate the effective emissivity of the wafer target to account for wafer emissivity and the chamber geometry, and its radiative properties. Using the temperature measurement equation with the estimated effective emissivity e_{eff}, an estimate of

the wafer temperature T can be determined from the observed spectral radiance temperature T_l,

$$\frac{1}{T} = \frac{1}{T_l} + \frac{l}{c_2} \ln e_{\text{eff}} \quad , \tag{1}$$

where l is the operating wavelength of the radiation thermometer and c_2 is the second radiation constant, 14,387.752 μm·K

The purpose of the present study is to establish the uncertainty of LPRT measurements for wafer temperature accounting for wafer and chamber characteristics. We present models for estimating the effective emissivity of the wafer that include effects due to wafer emissivity, shield reflectivity, light-pipe (LP) sensing tip area, and guard surface geometry and their radiative properties. Comparison of the TC and model-corrected LPRT temperature measurements are presented and the uncertainties of the LPRT calibration are described.

WAFER-CHAMBER ARRANGEMENT: THE RADIATION ENCLOSURE

The chamber of the NIST RTP tool has been described in detail in our companion paper [1]. The simplest model for estimating the effective emissivity of the wafer represents the wafer-shield arrangement as a 2-surface (infinite-parallel planes) enclosure. If the separation gap between the wafer and shield is very small, no appreciable temperature gradients exist across the wafer, and stray light from the heating lamps is minimal, then the model is appropriate. However, this model cannot account for the effects due to the cold (nearly black) sensing tip of the light pipe (LP) and the guard surfaces at temperatures quite different from the wafer. Figure 1 illustrates a more realistic model representing the wafer-chamber configuration by five regions forming an enclosure with multiple isothermal zones (24 total) located within two concentric, parallel circular disks and the lateral edge surface.

The five regions comprising the enclosure are as follows: (1) *Light Pipe* - The 4.3-mm diameter region (composed of the 2-mm diameter sapphire LP and the 3.8-mm diameter sheath) in the center of the reflective shield is modeled as cold and black; (2) *Reflective Shield* - The 200-mm diameter reflective shield not including the LP sensing tip area is assumed to be cold and diffuse (d) or specular (s) with reflectance of 0.799 or 0.993, respectively; (3) *Guard Tube* - The guard tube is the lateral cylindrical surface formed by a platinum-coated quartz tube of height equal to the gap separation, L. The guard ring is coplanar with the wafer. Both guard surfaces are assumed to be cold and black; (4) *LP Field of View* - The spot on the wafer corresponding to the field-of-view of the LP at the wafer, referred to as A_t, has the same characteristics as the rest of the wafer. The spot diameter D_t is dependent on the gap separation L and the LP diameter d = 2 mm according to the relation, $D_t = d + 2L/3$, which is based upon point-spread measurements of D_t for the LPRTs at several distances L form a point source. The variable D_t is defined as the diameter of the circle encompassing 99 % of the photocurrent from the LPRT; and (5) *Silicon Wafer* - The 200-mm diameter wafer (with a 3000 Å thermal oxide coating) is assumed to emit and reflect diffusely and have a uniform temperature. The spectral emissivity (0.955 μm) is assumed to be that for bare silicon [3] with a slight temperature dependence according to the empirical relation: $e_l = 0.691 - 5\times10^{-5}\times T(°C)$.

Measurements of the room-temperature, directional-hemispherical reflectance for the RTP chamber reflective shields and the silicon wafer were obtained using the NIST Spectral Tri-function Automated Reference Reflectometer (STARR) [4]. Reflectance measurements for the shields employed in this study are reported above. The room temperature spectral reflectance (0.955 μm) for the silicon wafers used in our study was measured as 0.686, which is in close agreement with the database [3] value at 30 °C of 0.680 from which the high temperature emissivity values were estimated.

EFFECTIVE EMISSIVITY MODELS

Two models are described for estimating the wafer effective emissivity for the five-zone enclosure shown in Figure 1. The first model treats the reflective shield as diffuse; that is, for a diffuse-gray enclosure. The second model treats the reflective shield as specular, while the remaining surfaces in the enclosure are diffuse.

Model with the Diffuse Shield

For the diffuse shield, the enclosure model is developed using the classical, radiosity method [5, 6] in which a radiation energy balance is written for

each surface (zone) A_i of the N-zone enclosure of the form,

$$\sum_{j=1}^{N}\left[\delta_{ij}-(1-\varepsilon_i)F_{i-j}\right]J_j=\varepsilon_i E_{bi} \quad , \tag{2}$$

where δ_{ij} is the Kronecker delta function, E_{bi} is the blackbody emissivity power, ε_i is the emissivity, J_i is the radiosity, and F_{i-j} is the diffuse radiation view (or exchange) factor defined as the fraction of radiation leaving A_i by emission and reflected irradiation that is intercepted by surface A_j. Using appropriate temperatures, emissivities and the N^2 view factors, the system of N equations is solved simultaneously to obtain the radiosities. The radiosity J_i represents the diffuse radiation leaving the surface A_i due direct emission *and* reflected irradiation resulting from intereflections within the enclosure. The effective emissivity ε_{eff} of the target area (t) is defined as the ratio of the target radiosity J_t to the blackbody emissive power $E_{b,t}$ at the temperature of the target area,

$$\varepsilon_{eff}=\frac{J_t}{E_{b,t}}=\frac{J_t}{\sigma T_t^4} \quad , \tag{3}$$

where the Stefan-Boltzmann constant σ is 5.67051×10^{-8} W/(m^2·K^4). Since the surfaces are gray, the total and spectral effective emissivities are equal, and this value is used in the temperature measurement equation, Equation (1), to determine the wafer temperature from the measured spectral radiance temperature.

An alternative analysis for the diffuse enclosure model is presented in the Appendix. Referred to as a generalized reflection method [7], the radiation energy balance requirement for each surface is written in terms of the spectral radiances, L_i, for the surfaces, their emissivities, and the relevant view factors. The two diffuse-enclosure methods of analysis are based upon the same assumptions (diffuse-gray surfaces), originate with surface radiation energy balances, and necessarily yield the same results. The radiosity method is widely practiced for heat transfer applications. The generalized reflectance method is more intuitive, but both are computationally tedious and comparable.

Model with the Specular Shield

For the specular shield, we have implemented the classical radiation transfer enclosure analysis for specular and diffuse surfaces [5]. In our model, all N surfaces of the enclosure emit diffusely, but the d diffuse surfaces (i = 1, 2, …, d; wafer and guard surfaces or zones) reflect diffusely and the (N - d) specular surfaces ($i = d$+1, d+2, …, N; the shield surfaces or zones) reflect specularly. For each diffuse surface, the radiation leaving the surface by direct emission and reflected irradiation is diffuse and is represented by the radiosity, J_i. For each specular surface, the only diffuse radiation leaving the surface is by emission, $\varepsilon_i E_{bi}$; the incident irradiation is specularly reflected. The transport between the surfaces based upon the radiosities J_i and emissive powers E_{bi} is determined by the *specular* exchange factor F^s_{i-j}, defined as the fraction of diffuse radiation leaving A_i that is intercepted by A_j by the direct path *and* by all possible paths involving intermediate specular reflections. Since the shield is planar and is the only specular surface in the enclosure aside from the direct path, there is just one additional path (no multiple specular reflections), thereby simplifying the evaluation of F^s_{i-j}. The energy balances for each of the diffuse surfaces forms a system of d equations that must be solved to determine the radiosity of target area,

$$\sum_{j=1}^{N}\left[\delta_{ij}-(1-\varepsilon_i)F^s_{i-j}\right]J_j=\varepsilon_i E_{bi}+(1-\varepsilon_i)\sum_{j=d+1}^{N}\varepsilon_j E_{bj}F^s_{i-j} \quad . \tag{4}$$

The effective emissivity of the wafer target follows from Equation (3) as with the diffuse case. Again, Equation (1) is used to determine the model-corrected LPRT temperature.

The radiation balances, Equations (2) and (4), for the enclosures with the diffuse and specular shield, respectively, were solved using 24 zones to represent the five regions earlier identified. Each zone is characterized by an area of uniform temperature and emissivity (or reflectivity). The wafer was represented by 10 concentric zones and the shield by 12 concentric zones. The guard ring and the guard tube were each represented by one zone. The resulting system of equations, with one equation for each radiation balance, was solved numerically for the radiosity J_i of each surface by using a standard LU decomposition method [8]. The radiosity of the

target J_t was divided by the known blackbody emissive power of the target to obtain the effective emissivity of the target area of Equation (3).

DISCUSSION OF RESULTS

We first discuss the results of a parametric study with the diffuse-shield and specular-shield enclosure models to demonstrate how the wafer effective emissivity is affected by wafer and shield radiative properties, gap separation, and LP sensing tip area. The models are used to correct the spectral radiance temperatures observed by the LPRT. An uncertainty analysis is performed for calibration of the LPRT directly to the ITS-90, and through the calibrated TCs described in our companion paper (see Figure 3, [1]).

The wafer effective emissivity e_{eff} estimated by the enclosure models for the diffuse (d) and specular (s) shields as a function of gap separation L for shields of different reflectance is shown in Figure 2. For these results, the LP sensing tip area is assumed to have the same properties as the shield. As expected, the effective emissivity increases with increasing shield reflectance. The effective emissivity for very small gap separations is only slightly dependent upon the diffuse-specular characteristics of the shield. For the condition $L \rightarrow 0$ mm, e_{eff} approaches the value predicted by an enclosure formed by two infinite-parallel planes. The diffuse-specular effect is more evident at larger gap separations, and the difference is larger with shields of higher reflectance. At L = 12.5 mm, a condition corresponding to the subsequent experimental data that will be examined later, the difference between the diffuse and specular shields ranges from 0.009 to 0.016 emissivity units, which amounts to 0.8 K to 1.2 K for the LPRT. We conclude that, for this condition, the diffuse and specular models give similar results.

In Figure 3, the diffuse-enclosure model shows the effective emissivity as a function of gap separation when the LP sensing tip has the reflectance of the shield (upper set of curves) compared to the conditions when the tip area is assumed as black. For the black LP tip condition, as $L \rightarrow 0$ mm, e_{eff} approaches the emissivity of the wafer. For very large gap separations, the influence of the LP tip radiative properties has minimal effect. At L = 12.5 mm, the LP tip condition has little influence, less than 0.01 emissivity units (less than 0.7 K), on the diffuse-model prediction for the effective emissivity.

The effective emissivity results in Figure 4 are based upon the diffuse model, assuming black LP tip areas of different diameters, for shields with reflectance of 99.3 % (specular) and 79.9 % (diffuse), which correspond to the shields employed in the experimental observations to be subsequently examined. Based upon the arguments developed in discussing Figures 3 and 4, we assume that the diffuse model is suitable to represent the specular-shield enclosure at a gap separation of 12.5 mm. Since the effect of LP tip diameter is more pronounced at smaller gap separations, we would expect that the differences between specular and diffuse behavior in this region to be significant, and that the results represent only expected general trends. At L = 12.5 mm, the influence of the LP tip diameter is only slightly more significant with the shield of higher reflectivity. Doubling the LP tip diameter from the 4-mm diameter, representative of the experiment conditions, to 8-mm diameter, reduces the effective emissivity by 0.016 and 0.012 emissivity units for the 99.3%-shield and 79.9%-shield, respectively. These emissivity changes amount to changes of 0.9 K and 1.2 K, respectively.

In Figure 4 of the companion paper [1], values of T_{tc}- T_l were observed with the 99.3 % specular shield and 12.5-mm gap separation under conditions when the shield-LP opening was 7 mm versus when the shield fit closely with the LP, about 4.3 mm diameter. The LPRT indicated temperature difference between these two conditions is about 6 °C to 9 °C, which is substantially larger than the diffuse model would predict. It would be more appropriate to use the specular model to analyze this condition since the shield is specular, and since the specular inter-reflections in the vicinity of the LP likely dominate the radiosity on the wafer target. However, the effect is more likely due to the larger chilling effect that a 7-mm black, cold opening causes relative to a 4-mm one.

Based upon the foregoing discussions, the diffuse-shield model, assuming the LP tip is black, is a suitable model for estimating the effective emissivity of the wafer with the specular and diffuse shield chamber arrangements of gap separation 12.5 mm. The model has been applied to the observed LPRT observations for these conditions as shown in Figure 3 of our companion paper [1]. The difference between the temperatures measured by the combination wire/thin-film thermocouple (TC), T_{tc}, and the model-corrected LPRT, T_{rad}, as a function of wafer temperature is shown in Figure 5. For the 99.3% (specular) shield, the difference amounts to about 1.3 °C, centered about zero difference, but with

an appreciable positive, near-linear trend. Overall, the agreement is within ± 0.6 °C. For the 79.9% (diffuse) shield, the difference trends are similar, but T_{rad} is systematically higher than T_{tc} by about 2 °C, implying that the model underestimates the effective emissivity of the wafer for this chamber arrangement.

Estimates for the uncertainties for the TC and LPRT measurements are shown in Table 1. The major contributor to the LPRT measurement uncertainty is the effective emissivity uncertainty. For the specular shield case, the effective emissivity is quite high, so that there is greater confidence in the model correction to the spectral radiance temperature than for the diffuse shield case. If we conclude that the uncertainty of the model effective emissivity amounts to 0.03 emissivity units, the corresponding uncertainty due to the effective emissivity uncertainty is about 2.0 °C. The second major contributor is due to the difference between the LPRT target and the TC thin-film junction amounting to 2.0 °C. The total TC and LPRT measurement uncertainties are 3.5 °C and 0.4 °C [1], respectively.

Table 1. Temperature uncertainties [°C] for comparison of LPRT and TC measurements.

LPRT measurements		TC measurements	
Calibration	0.2	TFTC (10 °C)	0.3
Effective emissivity	2.0	Pd/Pt TC	0.1
Junction/target temperature difference	2.0	TC emf	0.1
Temperature fluctuations	0.4		
Temperature drift	0.1		
LPRT display	0.1		
Subtotal	3.5	Subtotal	0.3

SUMMARY AND CONCLUSIONS

We have developed models of the wafer-chamber arrangements to estimate the effective emissivity of the wafer as a function of wafer and chamber radiative properties and chamber geometry. The effective emissivity estimates have been used to determine the wafer temperature from the observed spectral radiance temperature obtained with a light-pipe radiation thermometer (LPRT) calibrated on the ITS-90 against a blackbody. The total uncertainty for the LPRT temperature measurements, T_{rad}, was 3.5 °C; the uncertainty component due to the effective emissivity uncertainty estimated by the models was 2.0 °C. The total uncertainty for the thermocouple temperature measurements, T_{tc} , was less than 0.4 °C [1]. Comparison of the T_{tc} and T_{rad} measurements shows that they are in agreement within the prescribed uncertainties for the wafer temperature range 700 °C to 900 °C.

Under conditions when the model-corrected LPRT observations are used to determine wafer temperature using a blackbody calibration to the ITS-90, the uncertainty estimate is 3.5 °C. When the LPRT is calibrated against the calibrated thermocouple wafer [1], the uncertainty estimate is 2.1 °C. The latter method would be the preferred approach, assuming the wafer-chamber arrangement does not differ between the calibration condition and tool operating conditions. The benefit of the former method is that, a model if adequately validated, could be used to estimate uncertainties associated with different wafer emissivities and other changes to the wafer-chamber arrangement.

The diffuse- and specular-shield models provide understanding on the influence of wafer-chamber parameters and predict general trends for wafer effective emissivity. The models also provide useful estimates for determining wafer temperatures from LPRT spectral radiance temperatures. However, the models have not been able to explain the following experimentally observed chamber characteristics: effect of LP clearance hole (7 mm versus 4.3 mm); effect of gap separations at 6 mm and 9 mm; and temperature dependence of T_{tc} - T_{rad}. Refinement of the diffuse and specular models to accommodate more zones in the vicinity of the LP sensing tip, work currently in progress, could address some of these issues. Efforts to investigate surface temperature gradients, effects of the guard surface properties and temperatures, and the wafer temperature depression induced by the cold, black LP tip area are also under way. Designing experiments to critically validate the models, especially with good detail on the LP configuration, is yet another approach in progress to develop more confidence in model-correcting LPRT observations.

In this study we have demonstrated that in-tool calibrations against the ITS-90 with temperature uncertainties required by the SIA Roadmap are feasible. The new NIST combination wire/thin-film thermocouples on a silicon test wafer have calibrations with uncertainties less than 0.4 °C for the temperature range 650 °C to 920 °C. Using the test wafer as the reference source, we showed that light-pipe radiation thermometers can be calibrated against the ITS-90 with an uncertainty less than 2.1 °C for the conditions limited to the wafer-chamber

arrangement. Using classical enclosure modeling, accounting for wafer and chamber radiative properties and chamber geometry, the calibration uncertainty is less than 3.5 °C. More detailed models of the wafer-chamber radiation environment will improve our understanding on how to estimate effective emissivities with greater reliability and lead to improved calibrations for radiation thermometers used in production-styled RTP tools.

ACKNOWLEDGEMENT

The authors acknowledge with thanks the work of Professor Z. Zhang and his graduate students, F. Rosa and Y. Zhou, Department of Mechanical Engineering, University of Florida, Gainesville, FL, in developing the diffuse/specular enclosure analysis methods with support from the National Semiconductor Metrology Program, Office of Microelectronics Program, NIST.

REFERENCES

[1] C.W. Meyer, D.W. Allen, D.P. DeWitt, K.G. Kreider, F.L. Lovas, and B.K. Tsai, "ITS-90 Traceable Calibration of Radiometers using Wire/Thin-Film Thermocouples in the NIST RTP Tool: Experimental Procedures and Results," to be published in The 7th International Conference on Advanced Thermal Processing of Semiconductors, RTP '99, 1999

[2] F.J. Lovas, B.K. Tsai, and C.E. Gibson, "Meeting RTP Temperature Accuracy Requirements: Measurement and Calibrations at NIST," Rapid Thermal and Integrated Processing VII, Vol. 525, pp. 127-134, Materials Research Society, 1998

[3] J.P. Hebb, J.O. Cave, D. Wang, S. MacFarland, and K.F. Jensen, Multi-Rad, a PC based software package developed at the Massachusetts Institute of Technology with the sponsorship of SEMATECH (1997)

[4] P.Y. Barnes, E.A. Early, and A.C. Parr, "Spectral Reflectance," NIST SP250-48**,** 1998

[5] R. Siegel and J.R. Howell, Thermal Radiation Heat Transfer, Hemisphere Publishing Corporation, Washington 1992

[6] F. Rosa, Y.H. Zhou, Z.M. Zhang, D.P. DeWitt, and B.K. Tsai, "Modeling of the Radiation Environment in the Lower Chamber of Rapid Thermal Processing Furnaces," to be published in the proceedings of the 195th Meeting of the Electrochemical Society, Inc., 1999

[7] P. Saunders, "Reflection Errors in Industrial Radiation Thermometry", to be published in TEMPMEKO'99, The 7th International Symposium on Temperature and Thermal Measurements, Delft, The Netherlands, June 1-3, 1999

[8] W.H. Press, B.P. Flannery, S.A. Teukolsky, and W.T. Vettering, Numerical Recipes, pp. 31-38, Cambridge University Press, New York 1986

[9] Acharya, N. and P.J. Timans, "The Effect of Chamber Components on Wafer Temperature Response in an RTP System," Mat. Res. Soc. Symp. Proc., vol. 525, pp. 21-26, 1998

APPENDIX

GENERALIZED REFLECTION ENCLOSURE ANALYSIS FOR OBTAINING EFFECTIVE EMISSIVITY

In this section, a generalized reflection analysis is described for estimating the effective emissivity of a surface (the radiometer target area) in an enclosure comprised of N diffuse surfaces (zones). A generalized temperature measurement equation is written in terms of the target spectral radiance, blackbody spectral radiance, and effective emissivity. For each zone of the enclosure, an expression for the spectral radiance is written in terms of the zone characteristics, the spectral radiance of all the other zones, and the radiation view factors between the zones. The set of N equations is solved simultaneously to obtain the spectral radiances allowing the target effective emissivity to be determined.

Generalized Temperature Measurement Equation

Consider the enclosure of Figure 1. The LPRT (a spectral radiometer) viewing the target area (t) receives spectral radiance L_t equivalent to the blackbody spectral radiance at the spectral radiance temperature T_{lt} (the temperature indicated by the LPRT). These terms can also be expressed by the relation,

$$L_t = L_b\left(l, T_{l,t}\right) = e_{t,\text{eff}} L_b\left(l, T_t\right) \quad , \qquad \text{(A-1)}$$

where $L_b(l, T_t)$ is the blackbody spectral radiance at the true temperature of the target T_t. If the LPRT were provided with an instrumental emissivity setting, $\varepsilon_{t,eff}$ is the value of this setting that will correct for reflection effects causing $T_{l,t} = T_t$.

If the target were freely radiating (no inter-reflections between the wafer and its surroundings, as well as no irradiation from the surroundings), the effective emissivity would be equal to the emissivity of the target. For the target in our enclosure, Figure 1, the effective emissivity will be less than unity since there are no other surfaces in the enclosure at temperatures near that of the wafer and, the reflectance of the cold shield will be less than unity.

The generalized temperature equation, Equation (A-1) can be written in terms of temperatures using the Wien law to approximate the Planck blackbody distribution giving the more familiar expression of Equation (1).

Enclosure Analysis for Effective Emissivity

For each of the N zones (surfaces) in the enclosure of Figure 1, we can express the spectral radiance as the sum of the emitted component and a reflected component due to spectral radiances from the other zones (surfaces) in the enclosure.

$$L_i = e_i(l) L_b(l, T_i) + r_i \sum_{i=1}^{N} A_j F_{j-i} L_j / A_i \quad , \qquad \text{(A-2)}$$

In the second term, r_i is the reflectance of the i-th zone. The term $A_j F_{j-i} L_j / A_i$ represents the spectral radiance *incident* upon A_i due to radiant power (by emission and reflection) *leaving* A_j. The view factor F_{i-j} is the fraction of the radiant power that leaves A_i that is intercepted by A_j. For diffuse surfaces, the view factor is a function of the enclosure geometry only and can be evaluated using tabulated relations for common geometries or the integral relation explained in classical texts [5]. For each surface of the enclosure, the summation rule is

$$\sum_{i=1}^{N} F_{i-j} = \sum_{j=1}^{N} F_{j-i} \quad , \qquad \text{(A-3)}$$

and for any two surfaces in the enclosure, the reciprocity rule is

$$A_i F_{i-j} = A_j F_{j-i} \quad , \qquad \text{(A-4)}$$

Using the reciprocity rule, Equation (A-4) in Equation (A-2), the spectral radiance relation can be written as

$$L_i = e_i(l) L_b(l, T_i) + (1 - e_i(l)) \sum_{i=1}^{N} F_{i-j} L_j \quad , \qquad \text{(A-5)}$$

using the property relation for the opaque diffuse surfaces, $r = 1 - e$.

The spectral radiance relation of Equation (A-5) is written for each of the N surfaces in the enclosure forming a set of N equations that is solved simultaneously for the N unknowns. The target effective emissivity is then calculated from Equation (A-1) as

$$\begin{aligned} e_{t,eff} &= \frac{L_i}{L_b(l, T_t)} = \frac{e_1}{1 - (1 - e_1)(1 - e_2)} \\ &= \frac{e_1}{1 - (1 - e_1) r_2} \quad , \end{aligned} \qquad \text{(A-6)}$$

The energy balance relation of Equation 2, written in terms of the emissive power, radiosities, view factors and emissivity, is equivalent to the spectral radiance relation of Equation (A-5). The former, written for the total spectrum, assumes gray behavior, while the latter is written on a spectral basis. Both relations require that the surfaces are diffuse. The radiosity method for the classical diffuse-gray enclosure is widely used in heat transfer practice. The generalized reflectance method is conceptually less complicated and provides a convenient approach for determining the spectral effective emissivity of enclosures required for radiation thermometry applications.

A Simple Enclosure: Infinite, Plane-Parallel Surfaces

To illustrate the use of the generalized reflection method to estimate effective emissivity, consider two infinite, plane-parallel plates in an arrangement similar to Figure 1. The LPRT views the upper plate (1) of temperature and emissivity, T_1 and e_1,

respectively, through a small opening in the lower plate (2). The lower plate has an emissivity e_2 and is cold, $T_2 << T_1$ (and, consequently, $L_{l,\mathrm{b}}(l, T_2) << L_{l,\mathrm{b}}(l, T_1)$). Because the plates are planar, $F_{1\text{-}1} = F_{2\text{-}2} = 0$; and are of infinite extent, $F_{1\text{-}2} = F_{2\text{-}1} = 1$. Using Equation (A-5) above for each of the surfaces,

$$L_1 = e_1 L_b(l, T_1) + (1 - e_1)(F_{1-1} L_1 + F_{1-2} L_2) \quad , \qquad \text{(A-7)}$$

$$L_2 = e_2 L_b(l, T_2) + (1 - e_2)(F_{2-1} L_1 + F_{2-2} L_2) \quad , \qquad \text{(A-8)}$$

Solving the above set for L_1, the effective emissivity from Equation (A-6) has the form

$$\frac{L_1}{L_b} = e_{\mathrm{eff}} = \frac{e_1}{1 - (1 - e_1)(1 - e_2)} = \frac{e_1}{1 - (1 - e_1) r_2} \quad , \qquad \text{(A-9)}$$

where we have set $e_2 = 1 - r_2$. If surface 2 is the reflective cold shield, it follows that when $r_2 \to 1$, $e_{1,\mathrm{eff}} \to 1$. When the lower surface is cold and highly absorbing, $r_2 \to 0$ or $(1\text{-}e_2) \to 1$, it follows that $e_{1,\mathrm{eff}} \to e_1$; this is the condition where the upper surface is freely radiating (no inter-reflections with the surroundings).

This relation for the plane-parallel plates enclosure can also be obtained using the radiosity method. Acharya and Timans [9] use a flux model for radiation exchange to perform enclosure analysis for similar purposes.

Using Measured Spectral Radiances to Determine Effective Emissivity

Consider again the enclosure of Figure 1 representing the wafer-chamber arrangement with a hot wafer and cold reflective shield. Rather than having a single LPRT at the center, assume that additional LPRTs (say, 6 or 8) are positioned at uniform increments along the radial direction. This is a typical arrangement used in RTP tools. This array of LPRTs measure the spectral radiances, L_j (i = 1, …, N), (or equivalently, the spectral radiance temperatures) of targets along the wafer radial direction. These measurements can be used to compute the effective emissivities of the target areas and the wafer temperature at the target locations.

Combining Equation (A-5) with Equation (A-1), which defines the effective emissivity, in such a manner to eliminate $L_{\mathrm{b},i}\ (l,\ T_i)$, the effective emissivity of the target can be expressed as

$$e_{\mathrm{eff},i} = \frac{L_1}{L_{\mathrm{b},i}} = \frac{e_i(l)}{1 - [1 - e_i(l)] \sum_{i=1}^{N} F_{i-j} L_j / L_i} \quad , \qquad \text{(A-10)}$$

where the spectral radiance terms, L_j, are the measured values from the linear array of LPRTs. We need, of course, to define the zones such that they represent the target areas viewed by the LPRTs. Since the zones representing the shield and guard surfaces are cold, their spectral radiances will not appear in this equation, but their inter-reflections contributions are still considered.

Assuming that the wafer-chamber arrangement is properly represented by an enclosure model, this method of analysis provides a convenient approach for estimating the wafer temperature distribution based upon the measured spectral radiances (temperatures) at the LPRT locations.

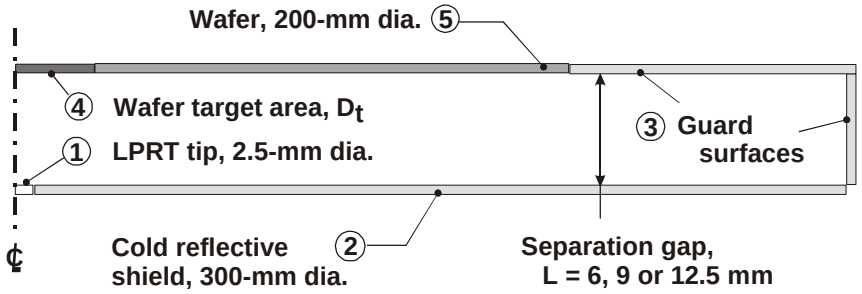

Figure 1. Cross-section schematic of the classical diffuse/specular enclosure representing the wafer-chamber arrangement in the NIST RTP tool.

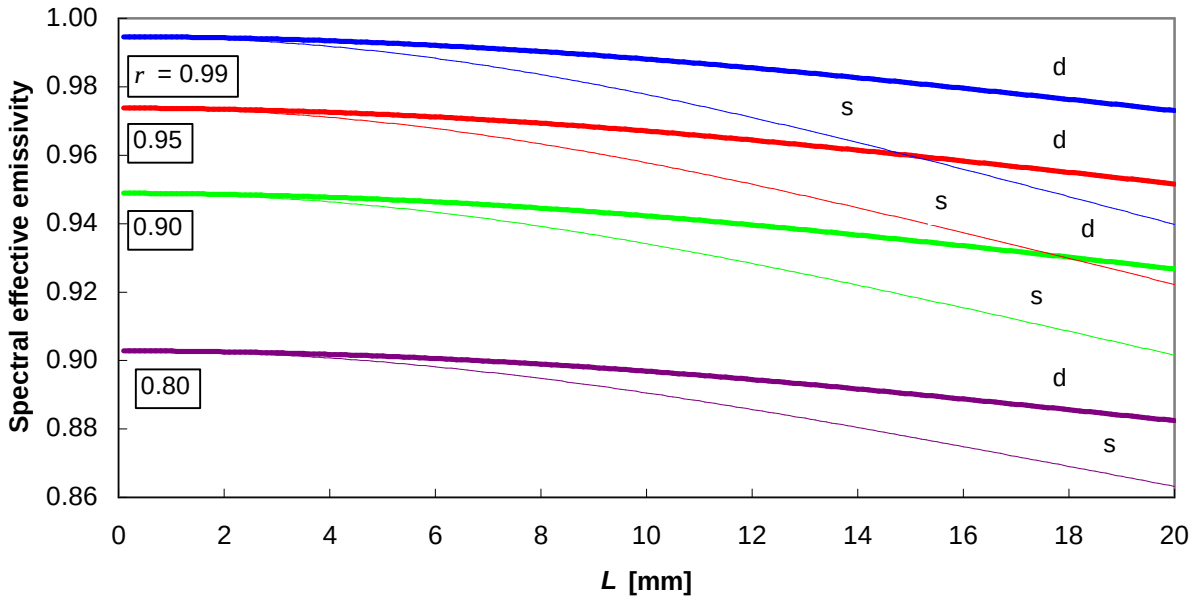

Figure 2. Wafer effective emissivity predicted by the 5-region, 24-surface enclosure models as a function of the gap separation *L* for diffuse (d) and specular (s) shields. The LP tip area has the same reflectance as the shield.

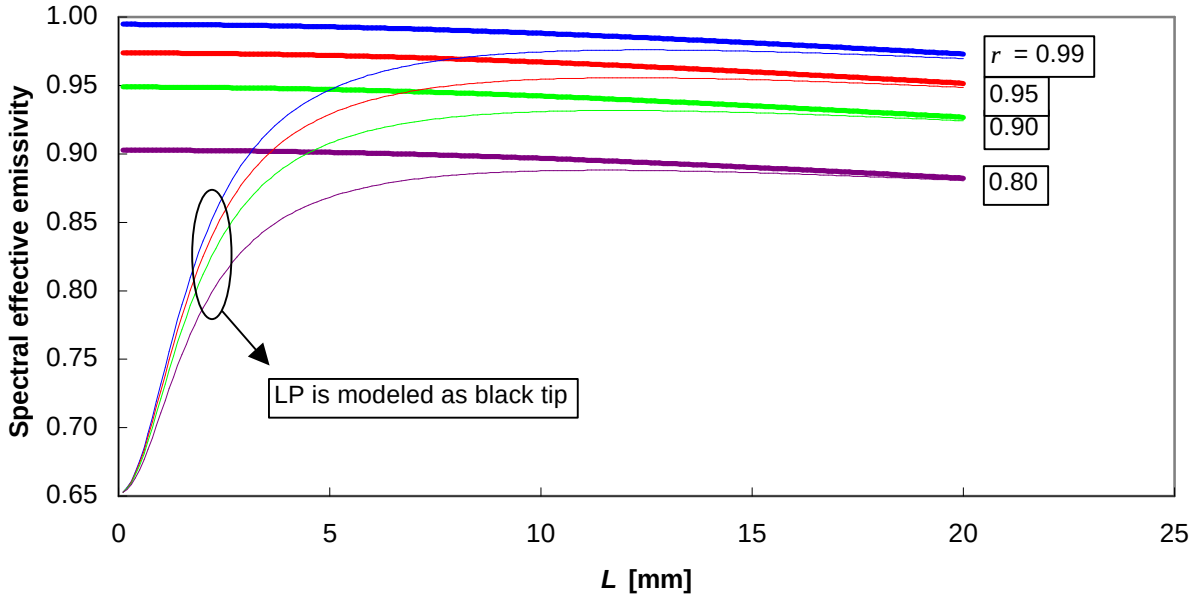

Figure 3. Comparison of wafer effective emissivity predictions from the enclosure model when the LP tip area has the reflectance of the shield versus when the LP tip area is black for diffuse reflective shields.

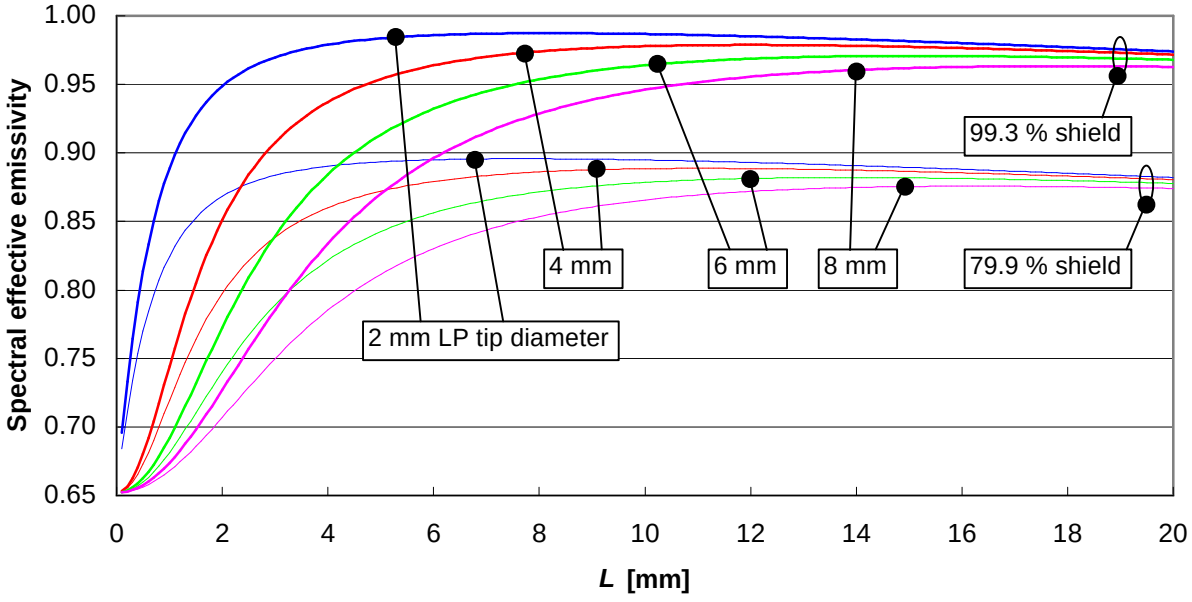

Figure 4. Comparison of wafer effective emissivity predictions for different LP tip diameters with best-fit experimental values based upon TFTC versus LPRT data with a diffuse shield of 79.9 % reflectance.

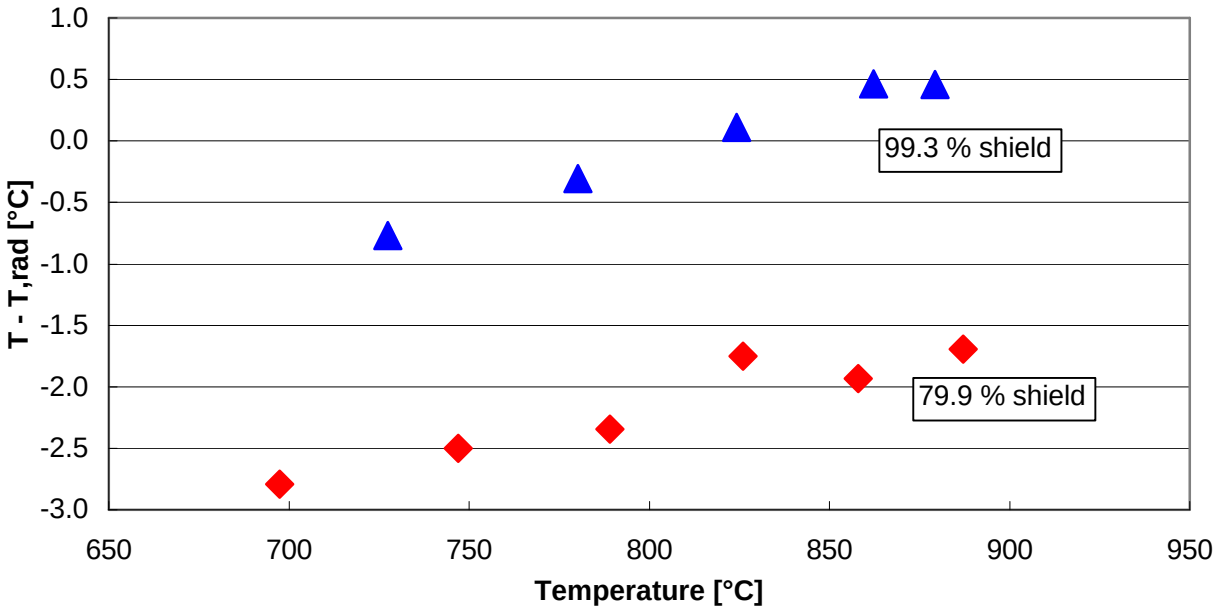

Figure 5. Comparison of TFTC and model-corrected LPRT wafer temperatures with the diffuse (79.9 % reflectance) reflective shield for a 12.5 mm gap separation.